Unraveling the Shape Transformation in Silicon Clusters

Koblar A. Jackson and Mihai Horoi
Physics Department, Central Michigan University, Mt. Pleasant, Michigan 48859, USA

Indira Chaudhuri and Thomas Frauenheim
Theoretische Physik, Universität-GH Paderborn, D-33098 Paderborn, Germany

Alexandre A. Shvartsburg
Pacific Northwest National Laboratory, MS K8-98, 3335 Q Avenue, Richland, Washington 99352, USA
(Received 11 December 2003; published 2 July 2004)

The prolate-to-spherical shape transition in Group IV clusters has been a puzzle since its discovery over a decade ago. Here we explain this phenomenon by elucidating the structures of Si_n and Si_n^+ with $n = 20$–27. The geometries were obtained in unbiased searches using a new "big bang" optimization method. They are substantially more stable than any found to date, and their ion mobilities and dissociation energies are in excellent agreement with experiment. The present results prove that the packing of midsize clusters is thermodynamically controlled and open the door to understanding the evolution of semiconductor nanosystems towards the bulk.

DOI: 10.1103/PhysRevLett.93.013401 PACS numbers: 36.40.Mr, 36.40.Wa, 36.40.Qv, 61.46.+w

Recent breakthroughs such as the discovery of luminescence in nanostructured [1] Si and the advent of Si photonic crystals [2] make clear the tremendous promise of traditional semiconductor materials when processed at nanometer scale. The key to future applications of semiconductor nanosystems is understanding their structure. In experiments, Si nanoparticles undergo a stunning prolate-to-compact shape transformation [3–6] over the 25–35 atom size range, which causes an abrupt change in physical properties such as cluster ionization energy [7]. While this transition was also observed in Ge and Sn clusters and is thus established as a general trait of semiconductor growth [6,8,9], the underlying molecular geometries have remained obscure despite a decade-long effort to determine them. Here we present structures for clusters with 20–27 atoms, a critical range spanning the onset of the shape transition. The geometries come from the big bang search algorithm, an unbiased and highly parallel method for searching cluster energy surfaces. These structures are significantly more stable than any found to date and neither resemble bulk Si packing nor obey the previous paradigm of tricapped trigonal prism (TTP) stacking [4,6,10–12]. The geometries are validated through independent comparisons to measured ion mobilities and dissociation energies.

Since the 1980s, structural characterization of silicon and other semiconductor clusters has been the focus of intense experimental and theoretical effort [4,6,11,12]. The geometries of the smallest Si_n were predicted via *ab initio* [13] and density-functional theory (DFT) [14] calculations on all conceivable isomers, yielding the triangle for Si_3, rhombus for Si_4, and bipyramids for Si_5–Si_7. They were verified by infrared [15] and Raman [16] matrix-isolation spectroscopies, and by anion photoelectron spectroscopy (PES) using the electronic transitions [17] and vibrational overtones [18]. Structures for slightly larger species arose from simulated annealing [14]: capped octahedra for Si_8 and Si_9 and TTP-based geometries for Si_{10} and Si_{11}. These are compact, multicoordinated geometries unrelated to the tetrahedral packing of bulk Si. At larger sizes, ion mobility spectrometry (IMS) revealed a remarkable structural transformation [3,5,6]: Si_n^+ clusters assemble in one dimension forming "sausages" up to $n \sim 25$, convert to near-spherical shapes over $n \sim 25$–35, and then grow three dimensionally towards mesoscopic Si particles. Understanding the shape transition hinges on elucidating the underlying molecular structures, yet numerous attempts to determine them have failed. An extensive genetic algorithm search located TTP-based geometries for $n = 12$–18. For $n = 19$ and 20, this gradient approximation approach produced compact structures, contravening the experimental data [4,6,11,12]. Later, a single-parent evolution (SPE) algorithm [19] found lower-energy prolate structures for Si_{19} and Si_{20}, but also fell short of the transition region. The geometries for $n \leq 20$ are now confirmed by multiple measurements: ion mobilities for cations and anions [6,12,19], dissociation energies and pathways for cations [19,20], ionization energies for the neutrals [11], and PES for anions [10]. For larger clusters in the transition region, a number of geometries have been obtained using diverse methodologies [21–24], but none has been vetted by direct comparison with experiment.

Below we identify Si clusters in the structural transformation region, up to 27 atoms. We obtained the geometries through extensive, unbiased searches of the energy surfaces, and tested them through direct, quantitative comparisons with all available experimental data. Since

 © 2004 The American Physical Society

earlier search methods failed [4,19] to get the right structures for $n > 20$, we developed a structural optimization tool termed "big bang." Its essence is to create random configurations of n atoms in a highly compressed space, typically $\sim 1/25$ of the normal molar volume. These supercompressed structures are allowed to "explode," relaxing to local minima via a standard gradient-based algorithm [25]. Millions of such minima are generated for each n by starting from different random geometries. Since all runs are independent, the process is inherently parallel. Starting from tightly packed geometries is critical, as searches with compression factors of ~ 1 proved ineffective. As the shapes of the local minima largely mirror those of the initial volumes (e.g., an elongated volume tends to produce prolate minima), searches for each size used several aspect ratios for the starting volume, allowing all possible shapes to emerge.

Performing millions of gradient minimizations for each size requires fast, yet accurate evaluation of energies and atomic forces. First-principles methods like DFT are too slow to do this directly, so we use a hierarchical approach that begins with the density-functional tight-binding (DFTB) method. DFTB closely approximates DFT, but runs $\sim 10^3$ to 10^4 times faster [26]. For each size, 200–400 of the best DFTB local minima are selected for investigation by DFT, here using the gradient-corrected Perdew-Burke-Ernzerhof (PBE) functional [27] and extensive basis sets (16 bare Gaussians, contracted to 6 s-type, 5 p-type, and 3 d-type functions on each atom). First, structures are ranked by DFT energy at the DFTB geometry. Then all isomers within ~ 0.5 eV of the ground state (~ 30 structures for each size) are relaxed to a precision of ~ 10 meV. The relaxation from the DFTB to DFT minima involves a roughly constant change in energy, so the ordering of DFT energies at the DFTB geometries is reliable. Since the DFTB was parametrized for neutral systems, searches were conducted for the neutrals. Low-energy Si_n^+ were found by removing an electron from all the Si_n isomers within 0.5 to 1 eV of the ground state, followed by full DFT relaxation of those within 0.4 eV of the bottom. The typical accuracy of the final energy ordering for either Si_n or Si_n^+ is 2–3 meV/atom.

Lowest-energy prolate and compact Si_n^+ geometries and the Si_n global minima ($n = 20$–27) are presented in Fig. 1. For both charge states, the best structures are significantly more stable than any previously known. By comparing relaxed geometries within PBE, we find the energy gain for the neutrals is 0.4–2.0 eV over Si_{21}–Si_{26} of Ho *et al.* [4], 0.5–1.0 eV over published Si_{21}, Si_{24}, and Si_{25} isomers [21–24], and 0.2–0.3 eV over the Si_{21} and Si_{22} obtained in SPE [19]. The Si_{20}^+ geometry is isoenergetic with that found previously [19], but matches the IMS data better (below). The preferred shape shifts as the clusters grow: compact Si_n^+ structures lie above the prolate for $n \leq 23$, closely compete with them for $n = 24$ and 25,

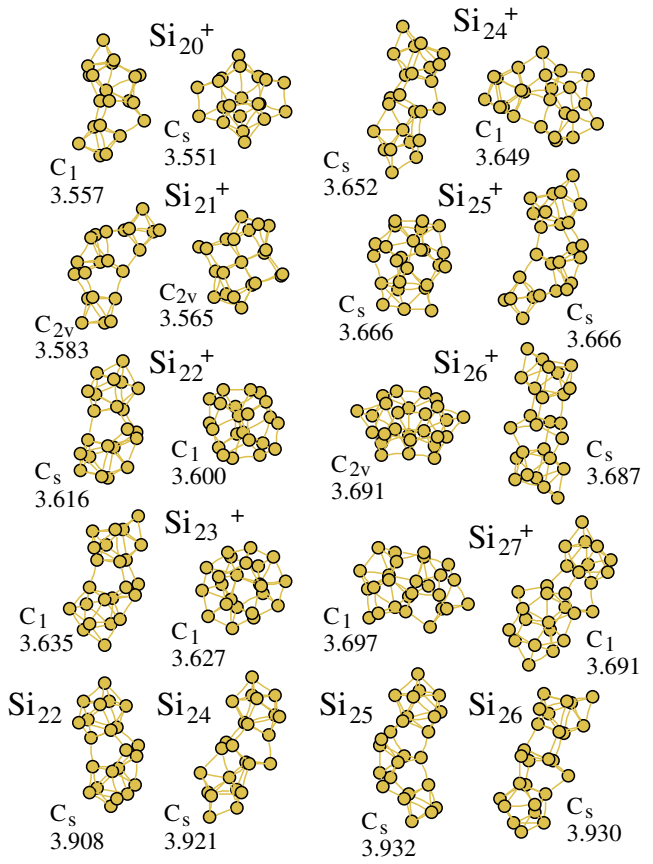

FIG. 1 (color online). Lowest-energy Si_n cations of prolate and compact families ($n = 20$–27) and the global minima for neutrals found in the "big bang" search. Cohesive energies (eV/atom) are listed. Ground states for Si_{21} and Si_{27} are identical to those for cations; Si_{20} and Si_{23} geometries have been reported [19]. The prolate Si_{22}^+ is the same as the published [19] Si_{22}, though a lower-energy neutral is found here.

and overtake them for $n \geq 26$. The transition in neutrals occurs a bit later: compact isomers become degenerate with prolate for Si_{26} and lower for Si_{27} (Fig. 1).

Our findings for Si_n^+ exactly mirror the IMS data [5], where compact Si_n^+ first appear at $n = 24$. In IMS, ion packets are pulled through an inert buffer gas (e.g., He) by an electric field [28]. This separates isomeric mixtures of mass-selected ions into components by ion mobility, depending on the orientationally averaged ion-buffer gas atom cross section. This quantity can be related to the ion geometry by classical molecular dynamics simulations [29,30]. This methodology has been used for Si_n ions up to $n = 20$ [4,6,11,19]. Experience shows that the mobilities computed for correct structures agree with experiment within $\sim 1.5\%$ and often better. (This error margin reflects the experimental error and estimated uncertainties in both the mobility calculations and the bond parameters of cluster geometries.) Calculations for our low-energy Si_n^+ isomers are compared with the measurements [5] in Fig. 2. The data in Ref. [5] feature multiple peaks at each cluster size across the transition

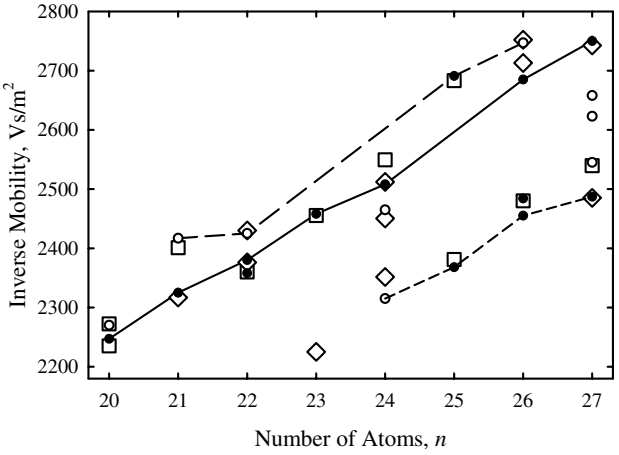

FIG. 2. Mobilities of Si_n cations in He (298 K). Circles stand for the measurements [5]: major peaks (filled circles) correspond to the most abundant isomers and minor peaks (empty circles) to less abundant isomers observed. Lines connect the structural families: "moderately prolate" (solid line), "stretched" (long dashed line), and "compact" (short dashed line). Squares and rhombi mark the values calculated for, respectively, the Si_n^+ global minima and other isomers within 10 meV/atom. When several geometries have nearly equal computed mobilities, only one symbol is shown.

region, and we indicate the positions of both major (most abundant isomers) and minor (less abundant isomers) peaks in the figure. The prolate clusters can clearly be grouped into two sequences [5]: "moderately" prolate structures that correspond to the major peaks at $n =$ 20–24, 26, 27 and "stretched" structures, corresponding to the major peak for $n = 25$ and minor peaks at $n = 21$, 22, and 26. The stretched structures for Si_{21}^+ and Si_{25}^+ shown in Fig. 1 are the first members of this family to appear in the literature; other low-lying prolate isomers for Si_{25}^+ are moderately prolate [22,23]. The compact family appears as a minor peak at $n = 24$ and includes the major peaks at $n = 25$–27.

The agreement between theory and experiment is exceptional for all three sequences, not just for all observed major peaks, but most minors as well, providing a quantitative explanation for most observed cases of polymorphism. For example, we found seven Si_{22}^+ isomers within 10 meV/atom of the ground state. Ranked by increasing energy, No. 1 and No. 5 fit the dominant "moderate" feature (see Fig. 2), No. 2, No. 3, and No. 4 match a smaller neighboring feature, and No. 6 and No. 7 match the minor "stretch" peak. At Si_{25}^+, there are two major peaks of equal height ("compact" and stretch) [5]. We find five Si_{25}^+ species that are degenerate within 2 meV/atom (with a 10 meV/atom gap to the next isomer) and all five match one of these two peaks. An apparent lack of polymorphism for Si_{23}^+ is also clarified by the calculations: all seven lowest-energy structures have nearly identical mobilities matching the lone experimental peak. Neutrals cannot be probed by IMS, but the structural transformation in Si_n^- happens 2–3 atoms later [5] than that in Si_n^+. This meshes well with our finding that the transition in Si_n neutrals is delayed by one or two atoms.

Consistency with IMS data does not suffice to establish structures: some high-energy Si_n morphologies ($n =$ 21–26) have correct mobilities [4]. Cluster energy is therefore a critical complementary criterion. While theory alone cannot guarantee that the bottom of a complex energy surface has been located, this can be determined by employing a "depth gauge" [20,31] based on measured cluster dissociation energies (E_D). The E_D for Si_n^+ can be defined as $E_D = E[n-m] + E[m^+] - E[n^+]$, where $E[n^+]$ is the total energy of Si_n^+, and m is chosen to minimize E_D. The ground states of the two dissociation fragments (Si_{n-m} and Si_m^+) are presumed known. Thus, if the search fails to recover the global minimum for Si_n^+, the predicted E_D falls short of the experimental value. The E_D computed for Si_n^+ ($n \leq 27$) and values measured by collision-induced dissociation [32] are compared in Fig. 3. The agreement is excellent, with all shortfalls under 0.3 eV—within the cumulative error margin of calculation and experiment. The greatest discrepancy is actually for a known geometry (Si_8^+). Significantly, the calculations reproduce the observed global minimum in E_D at Si_{21}^+. This trend differs drastically from that in "normal" nanosystems, where E_D increases monotonically with increasing size (save for local oscillations due to even/odd alternation and electronic or geometric shell closures). Figure 3 shows that our search has reached at least within a few meV/atom of the true ground states for all Si_n^+ up to $n = 27$. We have begun work on Si_{28}^+ and Si_{29}^+, but to date the E_D of our best geometries are still short of the targets by 0.4–0.6 eV (Fig. 3). This reflects the increasing complexity of the cluster potential energy surfaces with size and the challenge of conducting unbiased searches for the global minima.

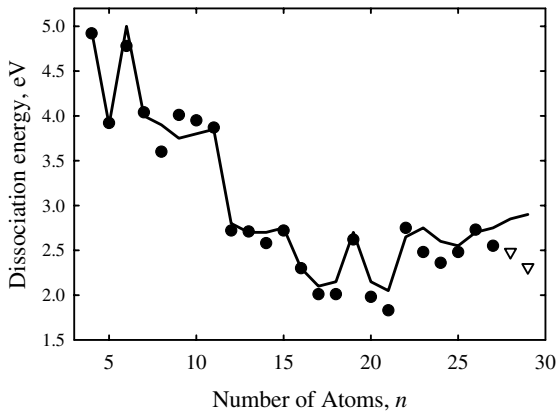

FIG. 3. Dissociation energies of Si_n cations. The line indicates the measurements [32]. The symbols are the values calculated for the Si_n^+ global minima found for $n \leq 27$ (circles) and our best structures to date for $n = 28$ and 29 (triangles).

The abnormal broad minimum in the dissociation energy at $n \sim 15$–25 and the global prolate-to-spherical transition have the same underlying cause and may be grasped in simple physical terms. The cause is the exceptional stability of several specific geometries for small Si clusters, most notably the Si_6 octahedron and Si_9 TTP. Initially, the lowest-energy pathway for cluster growth requires those uniquely stable structures to be retained as building units. This necessarily forces a cluster into a prolate shape, while E_D decreases and then levels on a plateau once the dissociation involves severing weak links between the units rather than breaking the units themselves. As the cluster grows such that some atoms could assume internal positions, the surface energy cost of prolate geometries outweighs the benefit of "special" subunits, inducing the transition to minimum-surface spherical shapes. Remarkably, the approximate size for this transition can be rationalized using the spherical drop model (SDM) [8]. With $\gamma = 740$ mN/m for the surface tension of liquid Si [33] and the bulk Si cohesive energy of 4.55 eV/atom, we calculate the energies of Si nanodroplets as $E(Si_{10}) = 3.78$ eV/atom, $E(Si_{20}) = 3.94$ eV/atom, and $E(Si_{30}) = 4.02$ eV/atom. Once these exceed the energies of the best prolate geometries (Fig. 1) at $n \sim 20$, clusters start rearranging into spherical shapes and the binding energy begins its ascent towards the bulk atomization enthalpy as prescribed by SDM. Since the smaller Si_n clusters are prolate, kinetic factors would favor the formation of prolate geometries even after the compact structures become more stable. However, the shape transition in experiments and the stability crossover found by the present global search coincide precisely. Thus, the cluster growth in this size range is controlled solely by thermodynamics.

In summary, new lowest-energy Si_n^+ geometries for $n = 20$–27 found by a blind search fit the whole body of ion mobility and dissociation energy data, and hence are almost certainly the structures observed through the shape transformation region. Prolate species still include Si_9 TTP units (e.g. Si_{23}^+ and Si_{25}^+), but not as ubiquitously as for $n = 13$–19 [4,12]. Instead, new building blocks appear: the Si_6 octahedron as in Si_{21}^+ and Si_{25}^+ and a sixfold ring (resembling that of an adamantane unit in bulk Si) bridging two subunits, as in Si_{24}^+. The compact structures for Si_{24}^+–Si_{27}^+ in Fig. 1 are the first compact geometries to be elucidated. These have neither the diamondlike packing of bulk Si, nor the stuffed fullerene structure with an outer shell of pentagons and hexagons suggested based on selected chemical reactivity data [34,35]. Surprisingly, some compact structures (e.g., Si_{24}^+) include TTP units that were believed to appear in the prolate species only. The present results bode well for using unbiased global optimizations to explore how the properties of silicon nanoclusters evolve toward the bulk, as well as to understand parallel structural transformations in other semiconductor systems.

We thank R. D. Smith and K. Tang for their support of IMS work at PNNL, D. Polovina, K. Chu, J. Boike, and J. Barra for computational assistance, and R. R. Hudgins and M. F. Jarrold for providing published IMS data. The support of NSF Grants No. DMR-RUI 99772333 and No. PHY-0244453 and DoE Grant No. DE-FG02-03ER15489 is acknowledged.

[1] K. D. Hirschman *et al.*, Nature (London) **384**, 338 (1996).
[2] S. Y. Lin *et al.*, Nature (London) **394**, 251 (1998).
[3] M. F. Jarrold and V. A. Constant, Phys. Rev. Lett. **67**, 2994 (1991).
[4] K. M. Ho *et al.*, Nature (London) **392**, 582 (1998).
[5] R. R. Hudgins *et al.*, J. Chem. Phys. **111**, 7865 (1999).
[6] A. A. Shvartsburg *et al.*, Chem. Soc. Rev. **30**, 26 (2001).
[7] K. Fuke *et al.*, J. Chem. Phys. **99**, 7807 (1993).
[8] J. M. Hunter *et al.*, Phys. Rev. Lett. **73**, 2063 (1994).
[9] A. A. Shvartsburg and M. F. Jarrold, Phys. Rev. A **60**, 1235 (1999).
[10] J. Müller *et al.*, Phys. Rev. Lett. **85**, 1666 (2000).
[11] B. Liu *et al.*, J. Chem. Phys. **109**, 9401 (1998).
[12] A. A. Shvartsburg *et al.*, J. Chem. Phys. **112**, 4517 (2000).
[13] K. Raghavachari, J. Chem. Phys. **84**, 5672 (1986).
[14] P. Ballone *et al.*, Phys. Rev. Lett. **60**, 271 (1988).
[15] S. Li *et al.*, Chem. Phys. Lett. **243**, 275 (1995).
[16] E. C. Honea *et al.*, Nature (London) **366**, 42 (1993).
[17] C. C. Arnold and D. M. Neumark, J. Chem. Phys. **99**, 3353 (1993).
[18] N. Binggeli and J. R. Chelikowsky, Phys. Rev. Lett. **75**, 493 (1995).
[19] I. Rata *et al.*, Phys. Rev. Lett. **85**, 546 (2000).
[20] A. A. Shvartsburg *et al.*, Phys. Rev. Lett. **81**, 4616 (1998).
[21] S. Yoo *et al.*, J. Am. Chem. Soc. **125**, 13 318 (2003).
[22] A. Sieck *et al.*, Phys. Status Solidi (b) **240**, 463 (2003).
[23] L. Mitas *et al.*, Phys. Rev. Lett. **84**, 1479 (2000).
[24] B.-X. Li *et al.*, Phys. Lett. A **316**, 252 (2003).
[25] D. C. Liu and J. Nocedal, Math. Prog. **45**, 503 (1989).
[26] D. Porezag *et al.*, Phys. Rev. B **51**, 12 947 (1995).
[27] J. P. Perdew *et al.*, Phys. Rev. Lett. **77**, 3865 (1996).
[28] M. T. Bowers *et al.*, Science **260**, 1446 (1993).
[29] A. A. Shvartsburg and M. F. Jarrold, Chem. Phys. Lett. **261**, 86 (1996).
[30] M. F. Mesleh *et al.*, J. Phys. Chem. **100**, 16 082 (1996).
[31] A. A. Shvartsburg *et al.*, Phys. Rev. Lett. **83**, 2167 (1999).
[32] M. F. Jarrold and E. C. Honea, J. Phys. Chem. **95**, 9181 (1991).
[33] H. Fujii *et al.*, Metall. Mater. Trans. A **31**, 1585 (2000).
[34] J. M. Alford *et al.*, J. Chem. Phys. **94**, 2618 (1991).
[35] U. Rothlisberger *et al.*, Phys. Rev. Lett. **72**, 665 (1994).